Radiology: Artificial Intelligence

TECHNICAL DEVELOPMENT

Improved Detection of Chronic Obstructive Pulmonary Disease at Chest CT Using the Mean Curvature of Isophotes

Peter Savadjiev, PhD • Benoit Gallix, MD, PhD • Morteza Rezanejad, PhD • Sahir Bhatnagar, PhD • Alexandre Semionov, MD • Kaleem Siddiqi, PhD • Reza Forghani, MD, PhD • Caroline Reinhold, MD • David H. Eidelman, MD • Ronald J. Dandurand, MD

From the Department of Diagnostic Radiology (P.S., S.B., A.S., R.F., C.R.), Research Institute (R.F., C.R., D.H.E., R.J.D.), Meakins-Christie Laboratories, Research Institute (D.H.E., R.J.D.), Centre for Innovative Medicine, Research Institute (R.J.D.), and Montreal Chest Institute (R.J.D.), McGill University Health Centre, 1001 Décarie Blvd, Montréal, QC, Canada H4A 3J1; Department of Pathology (P.S.), Medical Physics Unit, Department of Oncology (P.S.), School of Computer Science (P.S., K.S.), Department of Epidemiology, Biostatistics and Occupational Health (S.B.), Segal Cancer Centre and Lady Davis Institute for Medical Research, Jewish General Hospital (R.F.), and Department of Medicine (D.H.E., R.J.D.), McGill University, Montreal, Quebec, Canada; Institut de Chirurgie Guidée par l'Image, IHU Strasbourg, Strasbourg, France (B.G.); Bernhardt-Walther Laboratory, Department of Psychology, University of Toronto, Toronto, Ontario, Canada (M.R.); and Lakeshore General Hospital, Pointe-Claire, Quebec, Canada (R.J.D.). Received April 13, 2021; revision requested May 11; revision received November 17; accepted November 24. **Address correspondence to** P.S. (e-mail: *peter.savadjiev@mcgill.ca*).

P.S. supported by a Discovery Grant from the Natural Sciences and Engineering Research Council of Canada.

Conflicts of interest are listed at the end of this article.

See also the invited commentary by Vannier in this issue.

Radiology: Artificial Intelligence 2022; 4(1):e210105 • https://doi.org/10.1148/ryai.210105 • Content codes: AI CH CT

Purpose: To determine if the mean curvature of isophotes (MCI), a standard computer vision technique, can be used to improve detection of chronic obstructive pulmonary disease (COPD) at chest CT.

Materials and Methods: In this retrospective study, chest CT scans were obtained in 243 patients with COPD and 31 controls (among all 274: 151 women [mean age, 70 years; range, 44–90 years] and 123 men [mean age, 71 years; range, 29–90 years]) from two community practices between 2006 and 2019. A convolutional neural network (CNN) architecture was trained on either CT images or CT images transformed through the MCI algorithm. Separately, a linear classification based on a single feature derived from the MCI computation (called hMCI1) was also evaluated. All three models were evaluated with cross-validation, using precision-macro and recall-macro metrics, that is, the mean of per-class precision and recall values, respectively (the latter being equivalent to balanced accuracy).

Results: Linear classification based on hMCI1 resulted in a higher recall-macro relative to the CNN trained and applied on CT images (0.85 [95% CI: 0.84, 0.86] vs 0.77 [95% CI: 0.75, 0.79]) but with a similar reduction in precision-macro (0.66 [95% CI: 0.65, 0.67] vs 0.77 [95% CI: 0.75, 0.79]). The CNN model trained and applied on MCI-transformed images had a higher recall-macro (0.85 [95% CI: 0.83, 0.87] vs 0.77 [95% CI: 0.75, 0.79]) and precision-macro (0.85 [95% CI: 0.83, 0.87] vs 0.77 [95% CI: 0.75, 0.79]) relative to the CNN trained and applied on CT images.

Conclusion: The MCI algorithm may be valuable toward the automated detection and diagnosis of COPD on chest CT scans as part of a CNN-based pipeline or with stand-alone features.

Supplemental material is available for this article.

Chronic obstructive pulmonary disease (COPD) is clinically defined as airflow obstruction with respiratory symptoms as measured with spirometry (1,2). Traditionally, radiologic evaluation has not played a central role in the diagnosis of COPD. However, due to known limitations of spirometry in sensitivity to early disease (3,4), and given that objectively measured imaging markers of disease are important elements of optimal decision-making in clinical practice, there is an increasing interest in quantitative CT assessment of the lungs for disease detection, stratification, and risk prediction (5–9).

In medical imaging, convolutional neural networks (CNNs) have gained popularity and widespread use in recent years, and in chest CT analysis, they have been applied to the detection of COPD and other lung diseases (8–11). While CNNs have been shown to outperform other image analysis algorithms in a large variety of applications, recent computational developments have demonstrated that CNN performance can be improved if certain types of image geometry information are computed explicitly and input into the CNN, as this type of information is not readily available with standard convolution operations (12,13).

In this work, we introduce an image transformation that computes geometric information from CT images, specifically, the mean curvature of isophotes (MCI). Image isophotes (contours of equal luminance) and their properties have long been used in computer vision to capture geometric information important for image analysis and visual perception (14–16). To our knowledge, the application of MCI to chest CT scans has not previously been studied. Therefore, we investigate here the

Abbreviations

CNN = convolutional neural network, COPD = chronic obstructive pulmonary disease, GOLD = Global Initiative for Chronic Obstructive Lung Disease, hMCI1 = quantitative feature defined from distribution of voxel values in MCI images, MCI = mean curvature of isophotes, precision-macro = mean of per-class precision values, recall-macro = mean of per-class recall values, ROC = receiver operating characteristic

Summary

The mean curvature of isophotes is a classic computer vision technique that, when incorporated into a typical convolutional neural network pipeline or used on its own, may improve discrimination of chronic obstructive pulmonary disease at chest CT.

Key Points

- The mean curvature of isophotes (MCI) computes a geometric transformation on the original CT images.
- When trained on MCI images, a typical convolutional neural network (CNN) architecture sees improvement in precision and recall relative to the same architecture trained on the original CT images (McNemar test, $P < .001$).
- Simple threshold-based classification with a single histogram-derived feature from the MCI images matched the improved recall value of the CNN model.

Keywords

Chronic Obstructive Pulmonary Disease, Quantification, Lung, CT

hypothesis that COPD changes in the lung parenchyma can be reflected in the geometric properties of the image. Specifically, in this exploratory study, we test the hypothesis that training a CNN architecture on MCI images would result in a higher diagnostic performance for discriminating patients with COPD from controls, as compared with training the same architecture on the original CT images. We also test in a linear classification framework the discriminatory power of a single histogram-derived feature computed on the MCI images and compare its performance to that of the CNN.

Materials and Methods

Clinical Methods

This study was conducted with retrospective data acquired between 2006 and 2019 in patients with COPD and controls from two community-based pulmonology practices located in the West-Island suburbs of Montreal, Quebec, Canada (population 349 849), and Cornwall, Ontario, Canada (population 45 965). The study had institutional review board approval and patient informed consent was waived given the observational nature of the study. Using an initial database of 1160 patients, patients were included if they had undergone a non–contrast-enhanced CT scan and had pulmonary function test data available.

All patients with COPD had symptoms consistent with the disease, more than 10-pack-year tobacco use history, and satisfied the following Global Initiative for Chronic Obstructive Lung Disease (GOLD) spirometry criteria: either a forced expiratory volume in 1 second–to–forced vital capacity (or FEV_1/FVC) ratio of less than 0.7 (GOLD COPD stages 1–4), or a maximal midexpiratory flow of less than 65% predicted or a residual volume of greater than 130% predicted (pre-COPD) (2,4,17). Controls were drawn from the same practices, had fewer than 10 pack-years of tobacco use history, and had been determined to be free of respiratory disease following clinical and physiologic assessment.

In total, 274 individuals (31 controls and 247 patients with COPD) with CT scans acquired at eight different institutions were included. This sample included 151 women (mean age, 70 years; range, 44–90 years) and 123 men (mean age, 71 years; range, 29–90 years). CT scan data were imported into radiology software (OsiriX MD v.2.6; Primeo) for de-identification. Figure 1 summarizes our patient selection procedure.

CT Acquisition

A total of five different scanner models were used to image patients. Scanners and acquisition details are shown in Table 1.

Computational Methods Overview

An overview of the historical and mathematical background underlying the MCI algorithm is provided in Appendices E1–E3 (supplement). To assess the benefit of the MCI transformation, we compared the diagnostic performance of a CNN architecture trained on CT images to the performance of the same CNN architecture trained on MCI images. Separately, we also defined a simple quantitative feature from the distribution of voxel values in the MCI images (called hMCI1), and we used it to perform linear (threshold-based) classification. Details on image preprocessing are described in Appendix E4 (supplement). A description of the linear classification based on hMCI1 is given in Appendix E5 (supplement). Finally, a description on the development of the two CNN models trained with CT or MCI images is given in Appendix E6 (supplement), and a schematic illustration is provided in Figure E1 (supplement).

Statistical Analysis

We report the performance of all our models in terms of the mean of per-class recall values, called the *macro average of recall* (recall-macro), as well as the per-class average of precision (precision-macro). Use of these metrics allows for comparison to previous studies (8,9) and also mitigates the imbalance in sample size between our two classes. In a binary classification, recall is equivalent to sensitivity, and precision is equivalent to positive predictive value. Furthermore, the mean of per-class recall (recall-macro) is equivalent to the balanced accuracy (ie, to the mean of sensitivity and specificity).

The difference in classification performance between the CNN model trained and applied on CT images and the CNN model trained and applied on MCI images is assessed statistically via the McNemar test (18). The diagnostic performance of the two models was compared in four different contexts, each of which involves a binary discrimination: *(a)* the overall discrimination between controls and all patients with COPD; *(b)* between controls

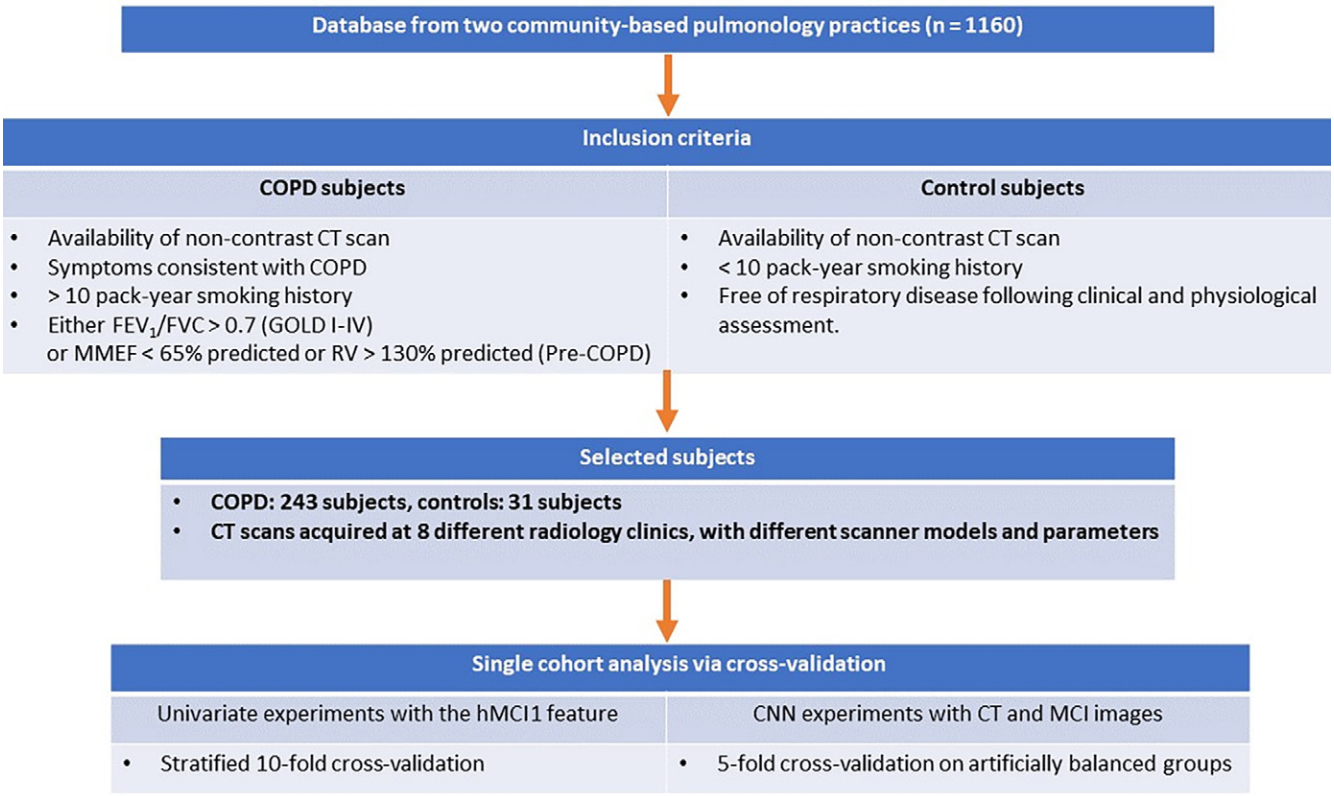

Figure 1: Flowchart summarizing patient selection and analysis. CNN = convolutional neural network, COPD = chronic obstructive pulmonary disease, FEV_1 = forced expiratory volume in 1 second, FVC = forced vital capacity, GOLD = Global Initiative for Chronic Obstructive Lung Disease, hMCI1 = quantitative feature defined from distribution of voxel values in MCI images, MCI = mean curvature of isophotes, MMEF = maximal midexpiratory flow, RV = residual volume.

Table 1: Technical Scan Parameters

	Scanner Model				
Parameter	Aquilion	Discovery CT750	LightSpeed VCT	Sensation 64	Somatom Definition Edge
Manufacturer	Toshiba	GE Medical Systems	GE Medical Systems	Siemens	Siemens
No. of scans*	1 (0.4)	25 (9)	232 (85)	14 (5)	2 (1)
Institution	A	B	C, D, E, F	B	G, H
Convolution kernel†	FC08 (1)	Lung (25)	Lung (1) Standard (231)	B70f (14)	B70f (1) I41f\3 (1)
Voltage (kV)‡	120	120	120	120	110 (100–120)
Tube current (mA)‡	234	103 (100–106)	266 (154–420)	248 (205–352)	125 (124–126)
Pixel spacing (mm)‡	0.65	0.70 (0.64–0.74)	0.69 (0.64–0.74)	0.67 (0.64–0.71)	0.80 (0.72–0.87)
Section thickness (mm)‡	1	2.5	1.25	3	2.50 (2.00–3.00)
Revolution time (sec)‡	NA	0.7	0.7	0.8	0.40 (0.30–0.50)
Spiral pitch factor‡	NA	0.98	1.38	1.38	0.78 (0.60–0.95)
Single collimation width (mm)	NA	0.63	0.63	0.63	0.6
Total collimation width (mm)	NA	40	40	40	38

Note.—NA = data not available.
*Data in parentheses are percentages.
†Data in parentheses are number of scans.
‡Data are presented as median with interquartile range in parentheses where values vary between CT scans.

and patients diagnosed as pre-COPD only; *(c)* between controls and patients diagnosed as GOLD stages 1–2 only; and *(d)* between controls and patients diagnosed as GOLD stages 3–4 only. In each of these four discrimination scenarios, the McNemar test was performed separately for each cross-validation fold, and we retained only the largest *P* value obtained over all folds. Given the

Table 2: Patient Characteristics and Spirometry

Parameter	Controls	Pre-COPD	GOLD 1	GOLD 2	GOLD 3	GOLD 4	*P* Value
Patient characteristic							
No. of patients	31	29	48	110	44	12	
Median age (y)	61 (51–71)	70 (65–79)	73 (67–78)	74 (69–78)	70 (64–78)	64 (58–73)	<.001
No. of women*	18 (58)	15 (52)	32 (67)	60 (54.5)	22 (50)	4 (33)	.35
No. of men*	13 (42)	14 (48)	16 (33)	50 (45.4)	22 (50)	8 (67)	
Tobacco use history (pack-years)	4.0 (0.0–13.5)	38.0 (29.0–44.0)	39.0 (27.8–47.5)	44.0 (33.2–53.0)	45.0 (34.0–54.2)	41.0 (36.2–66.5)	<.001
Height (cm)	166 (160–170)	164 (160–172)	159 (155–168)	164 (158–170)	164 (159–170)	166 (164–170)	.075
Weight (kg)	79 (70–88)	83 (66–99)	76 (65–86)	76 (67–88)	75 (58–87)	70 (64–87)	.66
BMI (kg/m^2)	28 (25–34)	30 (24–34)	28 (25–33)	28 (26–32)	26 (23–32)	26 (23–29)	.34
Spirometry							
No. of tests performed	29	29	48	110	44	12	
FEV_1 (L)	2.55 (2.19–3.47)	2.14 (1.58–2.49)	1.79 (1.54–2.41)	1.38 (1.16–1.73)	0.89 (0.76–1.10)	0.64 (0.51–0.68)	<.001
FEV_1 (% predicted)†	109 (97–115)	87 (80–106)	88 (85–95)	66 (59–73)	41 (37–46)	25 (20–27)	<.001
FVC (L)	3.19 (2.79–4.25)	2.81 (2.20–3.48)	2.88 (2.38–3.89)	2.61 (2.20–3.22)	2.38 (1.75–2.79)	1.96 (1.61–2.12)	<.001
FVC (% predicted)	107 (97–117)	100 (83–115)	116 (109–126)	96 (87–106)	78 (72–89)	59 (52–71)	<.001
FEV_1/FVC (%)	80 (78–84)	72 (71–73)	63 (61–66)	54 (49–59)	40 (36–46)	35 (30–38)	<.001
MMEF (L/sec)	2.78 (1.71–3.64)	1.36 (1.01–1.67)	0.87 (0.66–1.10)	0.51 (0.38–0.65)	0.29 (0.23–0.37)	0.23 (0.20–0.27)	<.001
MMEF (% predicted)	84 (65–107)	49 (43–60)	34 (27–39)	20 (15–25)	10 (9–13)	8 (7–9)	<.001

Note.—Except where otherwise noted, data are shown as median with interquartile range in parentheses. In each row, a *P* value resulting from a Kruskal-Wallis test indicates whether the groups differ in terms of the specified characteristic or spirometry variable. While the groups did not differ in terms of sex distribution, height, weight, and BMI, the individuals in the control group were younger than the patients classified as pre-COPD to GOLD stage 3 (post hoc Dunn test, $P < .005$) and GOLD stage 4 were younger than those classified as GOLD stage 2 (post hoc Dunn test, $P < .01$). By definition, forced spirometry differed between groups. BMI = body mass index, FEV_1 = forced expiratory volume in 1 second, FVC = forced vital capacity, GOLD = Global Initiative for Chronic Obstructive Lung Disease, MMEF = maximal midexpiratory flow.
*Data in parentheses are percentages.
†European Community for Steel and Coal–predicted values (19).

four reported *P* values (one for each discrimination scenario), a Bonferroni-corrected threshold of significance was set to .05/4 = .0125. The McNemar test was computed with the "mcnemar" function implemented in Python in the statsmodels package version 0.12.2 *(https://www.statsmodels.org/stable/index.html)*. Further details are provided in Appendix E6 (supplement).

Code

The code for our experiments is available at *https://github.com/petersv2/MCI_RadAI*.

Results

Clinical Characteristics

Demographic and clinical characteristics, as well as spirometry data, are provided in Table 2, with patients with COPD separated according to GOLD stage. In terms of racial characteristics, all patients are White with the exception of one Black and two Asian male patients.

Discrimination between the Control Group and Patients with COPD

For the simple univariate classification based on hMCI1 between controls and all patients with COPD, we report a receiver operating characteristic (ROC) curve analysis of classifier performance (Fig 2). The mean of area under the ROC curve across cross-validation folds was 0.87 ± 0.01 (standard deviation). The diagnostic performance of the linear classification based on hMCI1 was 0.85 (95% CI: 0.84, 0.86) for the recall-macro and 0.66 (95% CI: 0.65, 0.67) for precision-macro over the 10 folds of the stratified cross-validation.

Table 3 reports the discrimination performance of the two CNN models trained and applied on CT and MCI images,

as well as the statistical significance of the difference in their classification performance. All four *P* values obtained via the McNemar test were lower than the Bonferroni-corrected significance threshold of .0125.

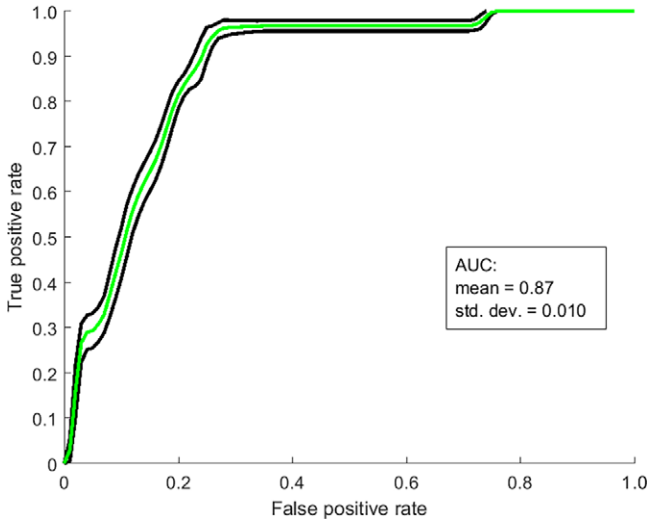

Figure 2: Classification between controls and all patients with chronic obstructive pulmonary disease using hMCI1 as a single feature in a linear classification model. Mean receiver operating characteristic (ROC) curve (green) computed over the 10 folds of stratified cross-validation. Black line shows ± 1 standard deviation (std. dev.) from the mean ROC curve. AUC = area under the ROC curve, hMCI1 = quantitative feature defined from distribution of voxel values in MCI images.

Additional results are presented in Appendix E7 and Figures E2–E4 (supplement), including visualization of MCI images and comparisons to quantitative CT metrics commonly used in the COPD literature.

Discussion

In standard clinical practice, COPD (and the subdivision of its severity into GOLD stages) is a diagnosis determined from clinical and physiologic tests, such as spirometry. The lack of a well-defined relationship between spirometry-based ground truth staging and radiologic appearance makes the automated image-based detection and staging of COPD challenging, even for powerful algorithms such as CNNs. In this study, we approached this challenge through the use of an image transformation that computes geometric information from CT images, specifically, MCI. Our results show that a CNN architecture trained on MCI images had higher diagnostic performance compared with the same CNN architecture trained on the original CT images; this trend was observed across all disease severity groups, including patients classified as pre-COPD. These findings support that CNNs do not always extract, on their own, all of the important information from an image, and may benefit from being provided geometric information relevant to tissue characteristics in a precomputed fashion, as shown in a small but growing body of literature (12,13).

It is likely that optimization of the CNN architecture and parameter tuning may have led to improved results with the CNN

Table 3: Diagnostic Performance of the CNN Models Trained and Applied on CT or MCI Images

Comparison	CT Images	MCI Images	*P* Value*
Control group vs all COPD			<.001
Recall-macro	0.77 (0.75, 0.79)	0.85 (0.83, 0.87)	
Precision-macro	0.77 (0.75, 0.79)	0.85 (0.83, 0.87)	
Control group vs pre-COPD			<.001
Recall-macro	0.75 (0.72, 0.78)	0.84 (0.80, 0.88)	
Precision-macro	0.62 (0.60, 0.64)	0.68 (0.65, 0.71)	
Control group vs GOLD stages 1–2			<.001
Recall-macro	0.77 (0.74, 0.80)	0.85 (0.82, 0.88)	
Precision-macro	0.76 (0.73, 0.79)	0.84 (0.81, 0.87)	
Control group vs GOLD stages 3–4			<.001
Recall-macro	0.77 (0.75, 0.79)	0.85 (0.82, 0.88)	
Precision-macro	0.69 (0.66, 0.72)	0.76 (0.73, 0.79)	

Note.—Diagnostic metrics, with 95% CIs in parentheses, computed over the cross-validation folds. For each of the four comparisons reported in the table, a *P* value was computed with the McNemar test to assess the significance of the difference in classification performance between the CNN trained and applied to CT images and the CNN trained and applied to MCI images. For each comparison, the McNemar test was performed separately for each cross-validation fold, and we report the largest *P* value obtained over all folds. Given the four reported *P* values, a Bonferroni-corrected threshold of significance is set to .05/4 = .0125. All the reported *P* values were below this threshold. CNN = convolutional neural network, COPD = chronic obstructive pulmonary disease, GOLD = Global Initiative for Chronic Obstructive Disease, MCI = mean curvature of isophotes, precision-macro = per-class average of precision, recall-macro = mean of per-class recall values.
**P* value shown for comparison between model trained with CT or MCI images performed with the McNemar test.

trained on CT images. In fact, one might argue that because of this lack of optimization, our CNN experiment on the original CT images may not be a good point of comparison to the CNN trained on the MCI images. To counter this argument, we note that the objective of this study was not to determine the most optimal CNN model for this specific clinical problem. Rather, it was to showcase the relative improvement in performance for the same CNN architecture and the same training algorithm when provided MCI images as input, as opposed to original CT images. In addition, our results were similar to those reported in previous studies. To our knowledge, there are only two recent studies on COPD detection using CNN-based analysis of CT images (8,9). Tang et al (9) used the ResNet CNN architecture. We used ResNet with 50 layers, whereas they experimented with 50, 101, and 152 layers. González et al (8) used a shallower network. Both studies used more complex preprocessing than ours, involving a selection of canonical sections or spatially corresponding regions to be compared across patients. Despite larger training sets, more advanced preprocessing steps, controlled acquisition protocols in all of the datasets involved, and a paucity of patients with early disease in some datasets (which should make discrimination easier), our results with a CNN on CT images were similar to their results. Depending on parameters (such as the number of layers in the ResNet architecture or a specific region of interest), the precision-macro and recall-macro values obtained by Tang et al (9) ranged from 0.69 to 0.76 and from 0.70 to 0.80, respectively. We obtained a value of 0.77 for both precision-macro and recall-macro (controls vs all COPD), toward the upper end of the range reported in Tang el al. The approach from González et al (8) results in recall-macro and precision-macro values of 0.77 for both measures (deduced from the confusion matrix in their figure 2A), which was very similar to our own results. We conclude that the diagnostic performance of our CNN architecture on CT images appears comparable to the current state of the art in the literature.

Our experiment with univariate classification based on the hMCI1 measure achieved the same recall-macro value of 0.85 as the CNN applied to MCI images, in a much simpler fashion. However, the precision-macro was lower at a value of 0.66. Nevertheless, this high recall value comparable to that of a CNN suggests this approach might be a viable and simple alternative to a CNN model in the context of screening for COPD. In such an application where recall is more important than precision, suspected COPD cases could be flagged, and those deemed uncertain can be flagged for further review by an expert to exclude potential false-positive findings. Screening for COPD is important for a variety of clinical reasons, including the initiation of tobacco use cessation, vaccination, and the prescription of medication to both relieve symptoms and treat exacerbations. Such strategies prolong lives and reduce health care costs (2).

Our study had limitations. As this was an exploratory study, our methods were not fully optimized, neither at the deep learning level, nor at the univariate classification level. For instance, we chose a threshold in the definition of hMCI1 in a somewhat arbitrary fashion, and we picked a fixed value of σ. In future work, instead of picking a threshold, we will work with the entire histogram data in combination with statistical techniques tailored to probability density estimates. We will also extend the approach to a range of spatial scales akin to classic scale-space approaches (14–16). Another limitation consisted of our small dataset, compared with other studies that worked with large prospectively acquired datasets (20–22). In future work, we will assess the performance of the MCI technique on large public prospective datasets (20–22). In the present study, we felt it was informative to present results on a retrospective sample derived from a community practice, as it emulates real-world clinical practice where data and conditions are less standardized compared with research cohorts. Another limitation stems from the lack of racial diversity among our patient population, with only three patients (1%) being non-White. In future work, this limitation will be addressed with validation on the above-mentioned prospective datasets (20–22), which are not only larger but also more racially and ethnically diverse.

As MCI has not previously been used in the context of disease prediction at chest CT, we performed a comparison between training the CNN on CT images alone versus MCI images alone, to evaluate the performance gain achieved by using MCI images compared with original CT images. In future work, a CNN could also be trained on both types of images simultaneously.

Whereas we have showcased the use of MCI in a discrimination context, an important next step is to identify the endophenotype(s) to which it is sensitive (23). Applying the technique to imaging data from explanted lung tissue samples with known characteristics could provide insight in that regard (24). In Appendix E7 (supplement), we discuss the spatial information inherent in MCI values and how it relates to specific structures in the lungs (see also Figs E2 and E3 [supplement]).

A potential application of using MCI images could be in detecting other diffuse lung disease, such as early interstitial lung disease. Currently, there is a lack of sensitive biomarkers with which to follow interstitial lung disease progression and monitor response to therapy (25). Preliminary data suggest that MCI potentially might also fill this unmet clinical need (26). In future work, we will investigate the ability of the MCI technique to differentiate between COPD, interstitial lung disease, and other types of lung disease. Finally, as the proposed MCI methods are organ and image modality agnostic, we plan to explore applications to other organs, diseases, and image modalities.

In summary, we evaluated the use of an image transformation, called the MCI, to discriminate COPD on CT images. Incorporated into a CNN analysis, this transformation allows an improvement in classification performance. Used instead in the context of a basic univariate classification, it still performs at a level that may be useful in certain types of applications. Further investigation of MCI images for classifying diseases at CT is warranted.

Author contributions: Guarantors of integrity of entire study, **P.S.**, **R.J.D.**; study concepts/study design or data acquisition or data analysis/interpretation, all authors; manuscript drafting or manuscript revision for important intellectual content, all authors; approval of final version of submitted manuscript, all authors; agrees to ensure any questions related to the work are appropriately resolved, all authors; literature research, **P.S.**, **K.S.**, **C.R.**, **R.J.D.**; clinical studies, **P.S.**, **B.G.**, **K.S.**, **C.R.**, **R.J.D.**; statistical analysis, **P.S.**, **M.R.**, **S.B.**, **K.S.**, **R.J.D.**; and manuscript editing, all authors.

Disclosures of conflicts of interest: P.S. Patent application *(https://patents.google.com/patent/US20190392579A1/)* under review, author is coinventor. **B.G.** Patent application *(https://patents.google.com/patent/US20190392579A1/)* under review. **M.R.** Funding for PhD studies from McGill University (School of Computer Science) under supervision of K.S.; Arts and Science postdoctoral fellowship from the University of Toronto; author's contribution to this work mainly from author's time as a PhD student at McGill University. **S.B.** No relevant relationships. **A.S.** No relevant relationships. **K.S.** Patent application *(https://patents.google.com/patent/US20190392579A1/)* under review. **R.F.** Clinical research scholar (chercheur-boursier clinicien) supported by the Fonds de recherche en sante du Québec (FRQS) and has an operating grant jointly funded by the FRQS and the Fondation de l'Association des radiologistes du Québec (FARQ); payment or honoraria from GE Healthcare (dual-energy CT, AI); method and system of performing medical treatment outcome assessment or medical condition diagnostic, contributor (5%), patent pending US20190392579A1. **C.R.** Contributor to patent *(https://patents.google.com/patent/US20190392579A1/)*. **D.H.E.** No relevant relationships. **R.J.D.** Contributor to patent *(https://patents.google.com/patent/US20190392579A1/)*.

References

1. Celli BR, MacNee W; ATS/ERS Task Force. Standards for the diagnosis and treatment of patients with COPD: a summary of the ATS/ERS position paper. Eur Respir J 2004;23(6):932–946.
2. Vogelmeier CF, Criner GJ, Martinez FJ, et al. Global Strategy for the Diagnosis, Management, and Prevention of Chronic Obstructive Lung Disease 2017 Report. GOLD Executive Summary. Am J Respir Crit Care Med 2017;195(5):557–582.
3. Woodruff PG, Barr RG, Bleecker E, et al. Clinical Significance of Symptoms in Smokers with Preserved Pulmonary Function. N Engl J Med 2016;374(19):1811–1821.
4. Regan EA, Lynch DA, Curran-Everett D, et al. Clinical and Radiologic Disease in Smokers With Normal Spirometry. JAMA Intern Med 2015;175(9):1539–1549.
5. Shaker SB, Dirksen A, Lo P, Skovgaard LT, de Bruijne M, Pedersen JH. Factors influencing the decline in lung density in a Danish lung cancer screening cohort. Eur Respir J 2012;40(5):1142–1148.
6. Kirby M, Tanabe N, Tan WC, et al. Total Airway Count on Computed Tomography and the Risk of Chronic Obstructive Pulmonary Disease Progression. Findings from a Population-based Study. Am J Respir Crit Care Med 2018;197(1):56–65.
7. San José Estépar R, Kinney GL, Black-Shinn JL, et al. Computed tomographic measures of pulmonary vascular morphology in smokers and their clinical implications. Am J Respir Crit Care Med 2013;188(2):231–239.
8. González G, Ash SY, Vegas-Sánchez-Ferrero G, et al. Disease Staging and Prognosis in Smokers Using Deep Learning in Chest Computed Tomography. Am J Respir Crit Care Med 2018;197(2):193–203.
9. Tang LYW, Coxson HO, Lam S, Leipsic J, Tam RC, Sin DD. Towards large-scale case-finding: training and validation of residual networks for detection of chronic obstructive pulmonary disease using low-dose CT. Lancet Digit Health 2020;2(5):e259–e267.
10. Walsh SLF, Calandriello L, Silva M, Sverzellati N. Deep learning for classifying fibrotic lung disease on high-resolution computed tomography: a case-cohort study. Lancet Respir Med 2018;6(11):837–845.
11. Ciompi F, Chung K, van Riel SJ, et al. Towards automatic pulmonary nodule management in lung cancer screening with deep learning. Sci Rep 2017;7(1):46479. [Published correction appears in Sci Rep 2017;7:46878.]
12. Clough JR, Oksuz I, Byrne N, Schnabel JA, King AP. Explicit Topological Priors for Deep-Learning Based Image Segmentation Using Persistent Homology. In: Chung A, Gee J, Yushkevich P, Bao S, eds. Information Processing in Medical Imaging. IPMI 2019. Lecture Notes in Computer Science, vol 11492. Cham, Switzerland: Springer, 2019; 16–28.
13. Rezanejad M, Downs G, Wilder J, et al. Scene Categorization from Contours: Medial Axis Based Salience Measures. In: 2019 IEEE/CVF Conference on Computer Vision and Pattern Recognition (CVPR), Long Beach, CA, June 15–20, 2019. Piscataway, NJ: IEEE, 2019; 4111–4119.
14. Koenderink JJ. The structure of images. Biol Cybern 1984;50(5):363–370.
15. Griffin LD, Colchester AC. Superficial and deep structure in linear diffusion scale space: Isophotes, critical points and separatrices. Image Vis Comput 1995;13(7):543–557.
16. Kuijper A, Florack LM. The relevance of non-generic events in scale space models. Int J Comput Vis 2004;57(1):67–84.
17. Han MK, Agusti A, Celli BR, et al. From GOLD 0 to Pre-COPD. Am J Respir Crit Care Med 2021;203(4):414–423.
18. Everitt BS. The analysis of contingency tables. London, England: Chapman & Hall, 1977.
19. Quanjer PH, Tammeling GJ, Cotes JE, Pedersen OF, Peslin R, Yernault JC. Lung volumes and forced ventilatory flows. Report Working Party Standardization of Lung Function Tests, European Community for Steel and Coal. Official Statement of the European Respiratory Society. Eur Respir J Suppl 1993;16:5–40.
20. Agusti A, Calverley PM, Celli B, et al. Characterisation of COPD heterogeneity in the ECLIPSE cohort. Respir Res 2010;11(1):122.
21. Bourbeau J, Tan WC, Benedetti A, et al. Canadian Cohort Obstructive Lung Disease (CanCOLD): Fulfilling the need for longitudinal observational studies in COPD. COPD 2014;11(2):125–132.
22. Regan EA, Hokanson JE, Murphy JR, et al. Genetic epidemiology of COPD (COPDGene) study design. COPD 2010;7(1):32–43.
23. Barnes PJ. Endo-phenotyping of COPD patients. Expert Rev Respir Med 2021;15(1):27–37.
24. Vasilescu DM, Martinez FJ, Marchetti N, et al. Noninvasive Imaging Biomarker Identifies Small Airway Damage in Severe Chronic Obstructive Pulmonary Disease. Am J Respir Crit Care Med 2019;200(5):575–581.
25. Wells AU, Brown KK, Flaherty KR, Kolb M, Thannickal VJ; IPF Consensus Working Group. What's in a name? That which we call IPF, by any other name would act the same. Eur Respir J. 2018;51(5):1800692.
26. Savadjiev P, Bhatnagar S, Semionov A, Dandurand RJ. A Computational Technique Based on the Mean Curvature of Isophotes for the Detection and Classification of Interstitial Lung Diseases on Chest CT. Am J Respir Crit Care Med 2021;203:A4599.